UNIVERSITY OF SCIENCE AND TECHNOLOGY OF HA NOI

INTERNSHIP REPORT

A STUDY OF THE THIRTY FOUR SOLAR FLARES DETECTED BY HA NOI AND LEARMONTH TELESCOPES AT 1415 MHz BETWEEN 2012 AND 2014

SUPERVISORS : Professor Pierre Darriulat

Doctor Nguyen Thi Thao

STUDENT : Nguyen Hoang Phuong Thanh

DEPARTMENT : Space and Application

INTAKE : 2013-2015

ACADEMIC YEAR : 2014

LABORATORY : Vietnam Astrophysics Training Laboratory

Ha Noi – August, 2014

CONTENTS

I. INTRODUCTION TO VATLY

The VATLY is abbreviated from **V**ietnam **A**strophysics **T**raining **L**aborator**Y.** It was created twelve years ago in the premises of the Institute for Nuclear Science and Technology in association with the Pierre Auger Observatory (PAO). However, it has moved its interest into radio astronomy recently.

A small radio telescope equipped with a 2.6 m diameter mobile parabolic dish remotely controlled in elevation and azimuth and with super-heterodyne detection around the 21 cm hydrogen line has been installed on the roof VATLY. After a period of running in, including measurements of the noise level and of pointing corrections, the excellent performance of the telescope had mapped neutral hydrogen in the disk of the Milky Way and obtained information on its arm structure and on the rotation curve of the Galaxy. It has currently being used to study the reflection of the Moon. VATLY has collaborated with IRAP in Toulouse and LERMA in Paris on the analysis of millimeter and sub-millimeter data. The IRAP collaboration uses data collected at the Plateau de Bure Interferometer Array on a remote (z=2.8) quasar gravitationally lensed by a galaxy in the foreground. Four images are detected in the continuum and on the red-shifted CO(7-6) line. Further studies will deal, in particular, with simulations and data related with ALMA, a large interferometer array recently constructed in Chile. The LERMA collaboration uses data collected at Nançay on CO (single dish) and at the Very Large Array on HI (interferometer) to observe the circumstellar shells of Red Giants on the Asymptotic Giant Branch, with particular emphasis on the study of the mass loss mechanism.

It is also training internship master students who spend two month in the lab and undergraduate students who spend four to six months to work on their dissertation at the end of their university years. Recent studies include: Global warming and cosmic rays; A study of diffusive shock acceleration in young Supernova remnants; The three body problem and formation of X-ray active binaries by capture and Gravitational Lensing and Einstein Rings.

II. REPORT

The present report relates work done in VATLY in summer 2014 in the context of a two month internship, in collaboration with my classmate Bui Van Tuan.

Chapter 1 collects material that was given to us by our supervisor for us to study, mostly lecture notes and encyclopaedia articles. During our stay in VATLY, each of us was asked to give a presentation of part of this material, Tuan on the general properties of the Sun and I more specifically on solar flares. Chapter 2 describes the reduction of the data on which Tuan and I worked together. The third chapter describes work which I did alone (Tuan was working on another subject).

1. THE SUN

1.1 General properties

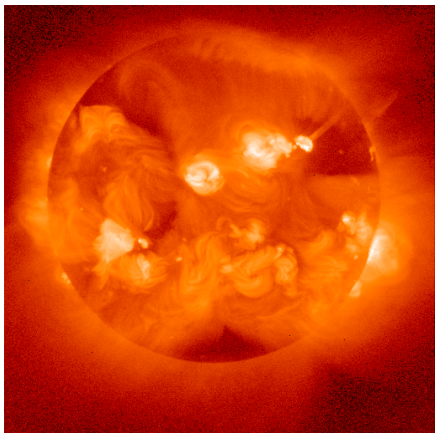

Figure 1.1. A radio picture of the Sun

The Sun, at the centre of the solar system, was born some five billion years ago from the gravitational collapse of a molecular cloud. It is located at 8.3 light-minutes (one astronomic unit by definition) from the Earth. It is a star of the Main Sequence with a surface temperature of ~5.8kK.

The Sun produces its energy by fusing protons into alpha particles. There are more than 10^{11} other stars in that state in the Milky Way. It consists of hydrogen (~ 74% in mass), helium (~24% in mass), and traces of other elements. Its spectrum displays lines of metallic atoms, ionised or neutral, and a few hydrogen line of weak intensity. The solar corona dilutes continuously at high temperature into space, producing the solar wind, a supersonic flux of charged particles that reaches a few hundred astronomic units (AU) away. It is in motion on a circular orbit around the centre of the Milky Way at a radius of some 25'000 light years at a speed of 250 km/s toward Cygnus (a full revolution takes 250 million years). The Sun will keep burning its hydrogen for another five billion years, after what it will become a Red Giant before its core collapse into a White Dwarf and its envelope fade away as a Planetary Nebula.

1.2 Structure of the Sun

The Sun is a yellow star of the Main Sequence making up some 99.86% of the total mass of the solar system. It is shaped as a nearly perfect sphere. It is made of plasma and rotates faster at the equator than at the poles. Rotation periods are 25.6 days at the equator and 33.5 days at the poles. However, as earth itself turns around the Sun, the mean rotation period seen from Earth is 28 days.

The Sun is a Population I star, therefore rich in heavy elements. It is probably the shock wave of one (or several) supernova that triggered the collapse of the cloud from which it is born, as suggested by the abundance of heavy elements, such as gold and uranium, which are very rare in Population II stars.

The edge of the Sun is somewhat smeared, density decreases exponentially as a function of radius in the vicinity of the surface. But it has a well-defined internal structure. The Sun radius is defined as that of the photosphere, meaning the layer above which gases are too cold or too diluted to radiate an important amount of light: it is the inner edge of this layer that can be seen by the naked eye.

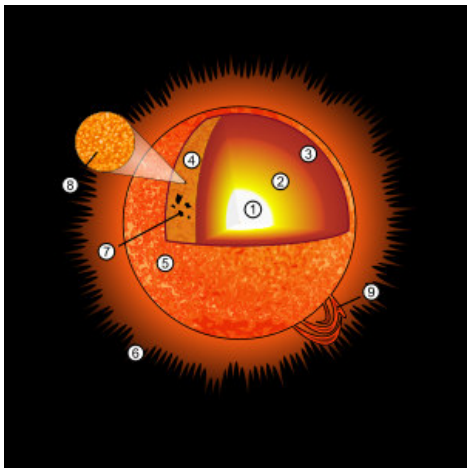

Figure 1.2. Structure of the Sun: 1. Core; 2. Radiative zone; 3. Convection zone; 4. Photosphere; 5. Chromosphere; 6. Corona; 7. Solar spots; 8. Granules; 9. Flares

The Sun interior is not directly observable and the Sun itself is opaque to electromagnetic waves. However, in the same way as seismology tells us about the inner structure of Earth from the seismic waves associated with earthquakes, helioseismology uses infrasonic pressure waves that travel inside the Sun to observe and measure its internal structure. Computer models of the Sun have been developed and make it possible to extrapolate the information down to its centre.

1.2.1 The core

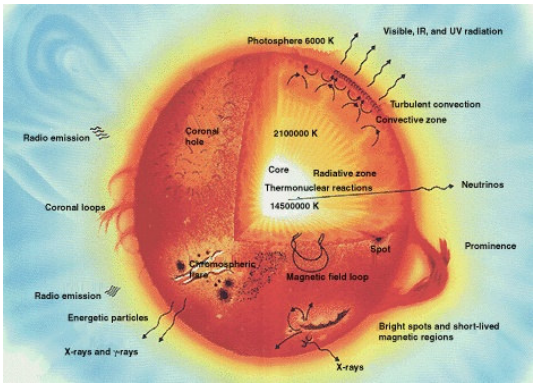

Figure 1.3. Schematic of the internal structure of the Sun

The core of the Sun reaches some 0.20 to 0.25 solar radii outward from the centre. It has a density of up to 150 g/cm^3 and a temperature nearing the million of Kelvin (while the Sun surface temperature is only 5.8 kK). During most of the star life, it produces energy by nuclear fusion in a sequence of reactions converting hydrogen into helium, the so-called p-p cycle. Less than 2% of the energy is produced via the CNO cycle. Nuclear energy is produced in the core exclusively: the rest of the star is simply heated by the heat that flows from the core outward to the surface. Before being released in outer space, this energy is several times absorbed and reemitted during its journey inside the star.

Each second, some 10^{38} protons are converted into helium nuclei (out of the ~10^{57} that the Sun contains). The mean power density is of the order of 0.2 mW/kg of matter, but the core power density is 150 times larger. As a comparison, the human body produces some 1.3 W/kg,

namely 600 times more than the Sun. The core power density is relatively low: only 0.27 W/m^3, namely much less than that of a candle. The nuclear fusion rate depends strongly on temperature and pressure, resulting in a stable equilibrium for the core: a small increase of the fusion rate increases the core temperature and makes it expand, thereby reducing the density and the fusion rate. Conversely a small decrease of the fusion rate induces a contraction and feeds back.

A few millimetres of solar plasma are sufficient to absorb the radiation produced by fusion, which is then reemitted isotropically at a slightly lower energy; the time it takes for the radiation produced in the core to reach the surface is very long, several tens of thousand years.

After having crossed the external convective layer, photons reach the external transparent layer and escape into space as visible light. A high energy photon produced in the core generates several millions of visible photons radiated this way. Fusion reactions produce also neutrinos that escape instantly because their interaction with matter is extremely weak.

1.2.2 Radiative zone

Between ~0.25 and ~0.7 solar radii, plasma is very hot and dense enough for the thermal radiation to transfer the produced heat outward. In this zone, although the temperature decreases with radius, (from 7 MK to some 2 MK), the temperature gradient is not sufficient for convection to play a significant role. Heat transfer is purely radiative – hydrogen and helium ions emit photons that are promptly absorbed before others be reemitted. Density drops by a factor 100 (from 20 g/cm^3 to only 0.2 g/cm^3) from the inner to the outer radiative zone.

Between the radiative and convective zones, there is an intermediate layer called tachocline. It is where one switches from a uniform rotation in the radiative zone to a differential rotation in the convective zone. Important shears result, successive layers sliding on top of each other. The fluid motion accelerates outward, producing magnetic field by dynamo effect.

1.2.3 Convective zone

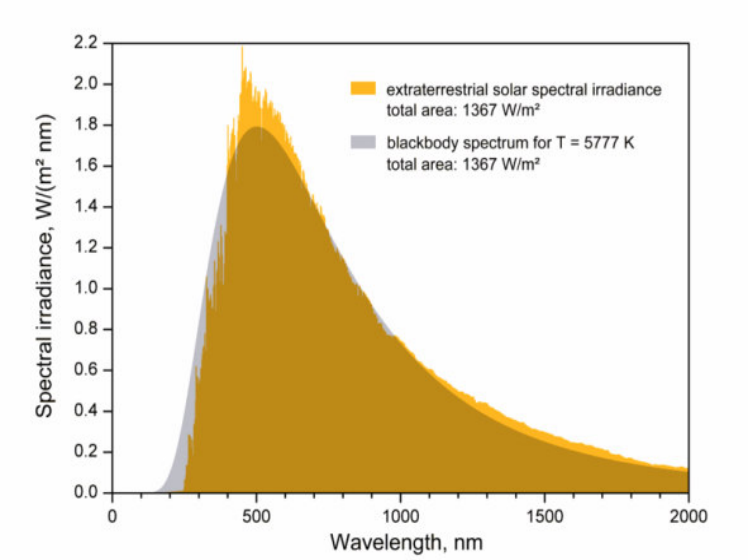

Figure 1.4. Solar spectrum compared with a black body spectrum.

In the external layer of the Sun, from 0.7 solar radii to the surface, plasma is no longer hot enough, nor dense enough, to transfer heat by radiation. It is the domain of convection, producing columns of heat exchange driving hot matter toward photosphere. As it reaches the surface, it cools down and dives again inward where it heats up when reaching the radiative zone. At the outer Sun radius, temperature has dropped to 5.7 kK and density to only 0.2 g/m^3.

The thermal columns of the convective zone imprint a kind of granulation on the solar surface. The associated turbulences generate a local dynamo effect producing magnetic dipoles on the whole surface.

1.2.4 Photosphere

The effective temperature, or black body temperature of the Sun, 5777 K, is the temperature that would have a black body of the same size that radiates the same power.

The photosphere, visible surface of the Sun, is the surface below which the Sun becomes opaque in visible light. Above the photosphere, visible light propagates freely into space and its energy is fully radiated. The change in opacity results from the decrease of H^- ion concentration: these ions are the main absorbers of visible light. Conversely, the light that reaches the Earth is dominantly produced by the interaction of electrons with hydrogen atoms, producing H^- ions. The thickness of the photosphere varies from several tens to several hundreds kilometres, corresponding to an opacity slightly smaller than that of the Earth atmosphere. The Sun light has a spectrum close to that of a black body superimposed on atomic lines radiated from the top of the photosphere. The photosphere has a density of ~10^{23} particles/m^3, namely ~1% of that of Earth at sea level.

1.2.5 Atmosphere

During a total solar eclipse it is possible to see the corona with the naked eye. The parts of the Sun above the photosphere are collectively called solar atmosphere. They are visible at all wavelengths, from radio to gamma rays. They include five main zones: the temperature minimum, the chromosphere, the transition region, the corona and the heliosphere. The latter, the higher solar atmosphere, reaches beyond Pluto's orbit to the heliopause where it forms an abrupt shock front at the border with interstellar matter. Chromosphere, transition region and corona are much hotter than the solar surface. This temperature rise is not well understood but is believed to be associated with Alfvén waves having enough energy to heat up the corona. The coolest layer of the Sun is that of the temperature minimum, some 500 km above the photosphere, with a temperature of some 4 kK, low enough to allow for the presence of some simple molecules such as CO and H_2O that are detected by their absorption lines. Above the minimum temperature layer, the chromosphere is some 2'000 km thick. It displays a characteristic spectrum with a rich set of emission and absorption lines. Its temperature increases progressively with altitude, reaching some 20 kK at the top, where helium is partially ionised.

Figure 1.5. Total solar eclipse revealing the corona.

Above the chromosphere, the transition region is only 200 km thick. Its temperature increases steeply to near the million K in the corona. This increase is due in part to the full ionization of helium in the transition region, significantly reducing the radiative cooling action of the plasma. The altitude of the transition region is not well defined. It consists in halos embedding turbulences of the chromosphere, spicules or filaments, and is the seat of a constant chaotic motion. It is difficult to observe it from ground, but it can easily be studied from space using detectors sensitive to the far UV.

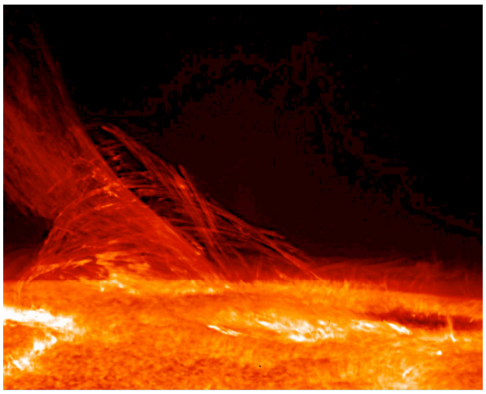

Figure 1.6. Picture taken by the Hinode's Solar Optical Telescope on January 12th 2007. It reveals the filamentary nature of the plasmas connecting regions of different magnetic polarities.

The corona is the higher part of the solar atmosphere, embedding a volume much larger than that of the Sun as such. It expands into space to generate the solar wind that fills the whole solar system. The lower part of the corona, near the Sun surface, has a density of 10^{15} to 10^{16} particles/m^3. The mean temperature of the corona and solar wind is between 1 and 2 MK, reaching 8 to 20 MK in the hottest regions. We lack a theory accounting for the corona temperature but one knows that part of the heat it receives is related to magnetic reconnections.

The heliosphere, which includes the solar wind, covers from some 20 solar radii (0.1 AU) to the extreme limits of the solar system. Its inner boundary is defined as the place where the solar wind flux becomes *superalfvénic* – namely faster than Alfvén waves. Turbulences and other movements that occur beyond this limit cannot act on the corona because the speed of transmission of a signal cannot exceed Alfvén velocity.

1.3 Magnetic field

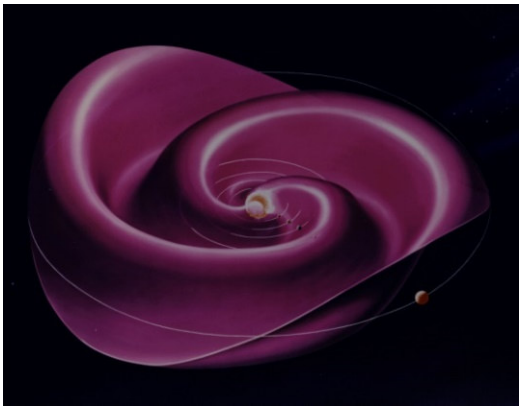

Figure 1.7. Spiral structure of the solar magnetic field.

The solar wind escapes radially in the heliosphere, producing a spiralling magnetic field – because of the solar rotation – that extends to more than 50 AU from the Sun. This rotating magnetic field acts on the currents generated by the plasma motion within the heliosphere.

1.3.1 General features

The Sun is a magnetically active star. It is the seat of a strong and variable magnetic field, that evolves from one year to the next and changes polarity every eleventh year when reaching its maximal activity. This magnetic field is the result of many effects collectively called solar activity. It covers solar spots, fluctuations of the solar wind, flares and major coronal ejections. On Earth, it cause auroras and perturbs electric energy networks as well as radio wave transmission. One thinks that solar activity plaid an important role in the formation and evolution of the Earth via the changes that it induces in the structure of the upper atmosphere.

The dependence of the rotation velocity on latitude causes the dynamo effect by winding field lines that get closer and closer up to producing solar spots and flares before reconnecting and changing polarity. The length of this cycle is about eleven years.

1.3.2 Solar flares

Solar flares were first observed on the Sun by R. C. Carrington and independently by R. Hodgson in 1859 as localized visible brightening of small areas within a sunspot group. A solar flare is a sudden flash of brightness observed over the Sun's surface or the solar limb, which is interpreted as a large energy release of up to 6 10^{25} J of energy (about a sixth of the total energy output of the Sun each second). They are often, but not always, followed by a colossal coronal mass ejection (CME): the flare ejects clouds of electrons, ions, and atoms through the corona of the Sun into space. These clouds typically reach Earth a day or two after the event. Solar flares affect all layers of the solar atmosphere (photosphere, chromosphere and corona); the plasma medium is heated to tens of millions of kelvins (several keV, up to MeV scale) and electrons, protons, and heavier ions are accelerated. While an electron having a kinetic energy of 1 MeV has nearly the speed of light, a proton having a kinetic energy of 1 MeV has a momentum of ~45 MeV/c, meaning a velocity of ~4.5% of the speed of light. They produce radiation across the electromagnetic spectrum at all wavelengths, from radio waves to gamma rays; most of the energy is spread over frequencies outside the visual range and for this reason the majority of the flares are not visible to the naked eye and must be observed with special instruments. Flares occur in active regions around sunspots, where intense magnetic fields penetrate the photosphere to link the corona to the solar interior. Flares and CMEs are powered by the sudden (timescales of minutes to tens of minutes) release of magnetic energy stored in the corona. Magnetic reconnection occurs when the density of field lines becomes too high. The sudden release of energy in this reconnection is the origin of the particle acceleration. This explains why solar flares typically erupt from what are known as the active regions on the Sun where magnetic fields are much stronger on average. The frequency of occurrence of solar flares varies, from several per day when the Sun is particularly active to less than one every week when the Sun is quiet, following the 11-year cycle.

Flares can affect Earth's ionosphere and disrupt long-range radio communications. They strongly influence the local space weather in the vicinity of the Earth. They can produce streams of highly energetic particles in the solar wind, which can impact the Earth's magnetosphere, and present radiation hazards to spacecraft and astronauts. Additionally, CMEs can trigger geomagnetic storms that have been known to disable satellites and knock out terrestrial electric power grids for extended periods of time. Energetic particles in the magnetosphere contribute to auroras.

1.3.3 Interplanetary field

The solar magnetic field extends much farther out than the Sun. The solar wind, a plasma in which the field is anchored, carries magnetic field in the whole solar system, one talks of the interplanetary field. As the plasma moves along the field lines, the interplanetary field is radial near the solar surface. As the magnetic field has different polarities in the northern and southern hemispheres, there exists near the solar equator a thin current layer, the heliospheric current. Away from the Su, the field lines wind up in an Archimedes spiral, called Parker spiral. The interplanetary field is much stronger than the dipole component of the solar magnetic field. The latter reaches between 50 and 400 μT in the photosphere, and decreases as the distance cubed to reach 0.1 nT at the level of the Earth orbit, where however the interplanetary field is hundred times stronger, reaching some 5nT.

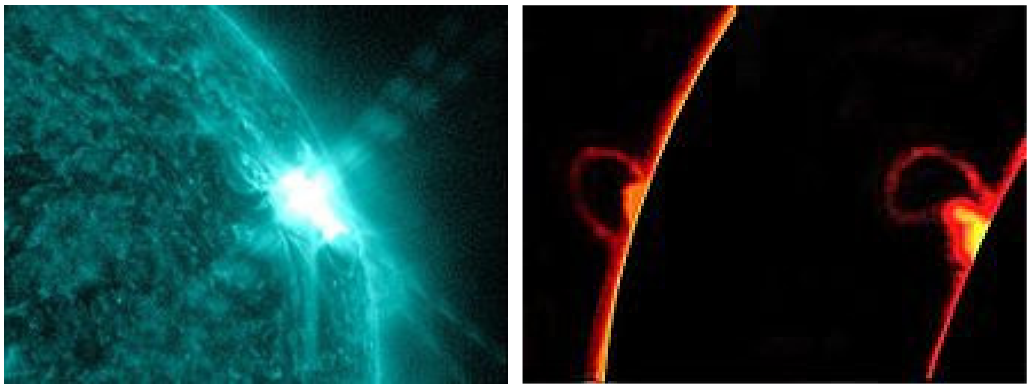

Figure 1.8. Left: An M7.9 class Solar Flare. Right: Two successive photos of a solar flare phenomenon. The solar disc was blocked in these photos for better visualization of the flare's accompanying protruding prominence.

The superposition of the Earth dipole on the interplanetary field produces the Earth magnetosphere. Its structure is complex. In particular the higher density of field lines near the poles trap the solar wind particles to produce auroras.

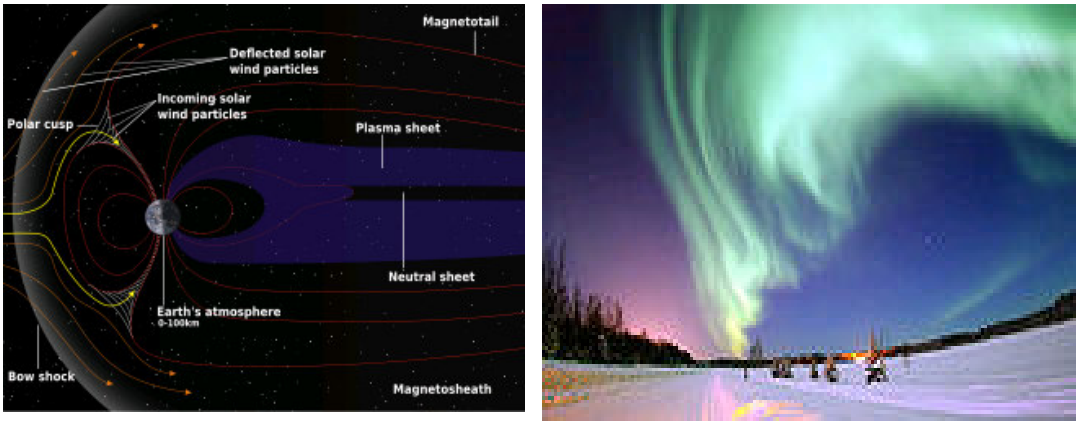

Figure 1.9. Schematic structure of the magnetosphere (left) and picture of an aurora (right).

1.3.4 Solar spots and solar cycle

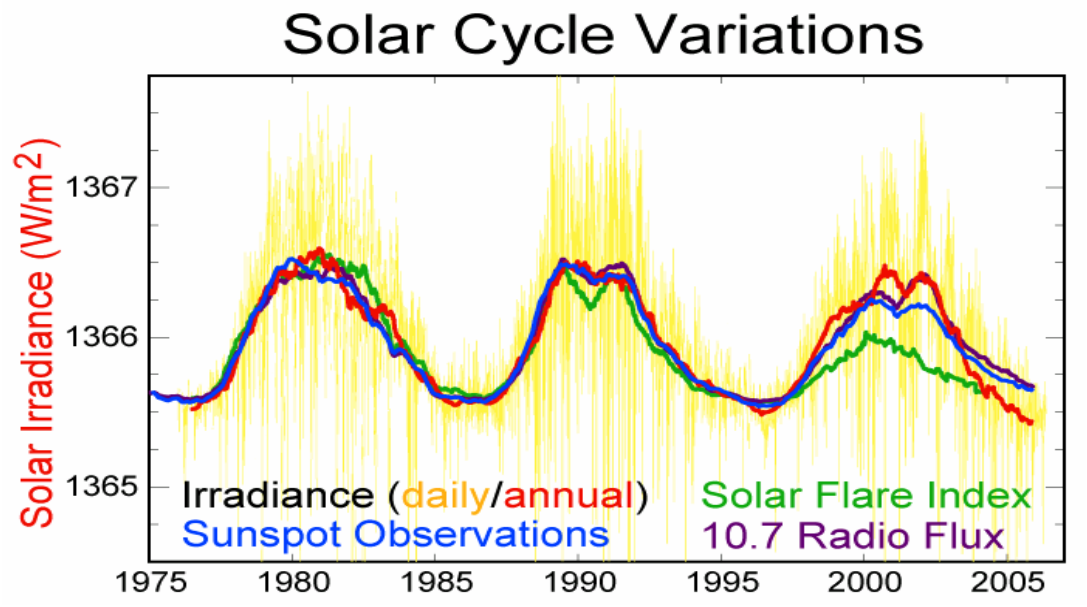

Figure 1.10. The three most recent completed solar cycles.

When one observes the Sun with proper filters, one immediately notices the presence of spots. These are well defined regions that are darker than their surrounding because they are less hot. They are areas of intense magnetic activity preventing convection to take place and therefore reducing the amount of heat transferred from the interior to the surface. The result is a strong heating of the corona, going together with solar eruptions and coronal mass ejections. The larger spots reach thousands of kilometres in diameter.

The number of solar spots follows the eleven years cycle. Typically, at activity minimum, one sees only very few spots, or even none. Then, as activity increases, spots appear first at large latitudes, then closer and closer to the equator (Spörer law). Spots are usually grouped in pairs of opposite magnetic polarities.

1.3.5 Anomalies

The solar cycle has an important impact on climate, the Sun luminosity being related to its magnetic activity. Minima lasting longer than average tend to be associated with higher Earth surface temperatures. During the XVIIth century, the solar cycle paused for several decades and very few spots were observed during what is called the Maunder minimum or small ice period. Europe then experienced very low temperatures. Other similar minima have been revealed by the study of the tee growth circles.

It so happens that the Sun currently shows some anomalies: while the solar wind and the magnetic field that it carries more than doubled during the past century, it now experiences solar spot minima lasting longer than usual. During the past two decades, the speed of the solar wind has decreased by 3%, its temperature by 13% and its density by 20%. Before the recent surge of activity, its magnetic field was twice as weak as 22 years before. The current maximum is lower than those preceding (Figure 1.12). A result is a decrease of the volume of the heliosphere and an increase of the flux of cosmic ray reaching the Earth. Such anomalies are not understood.

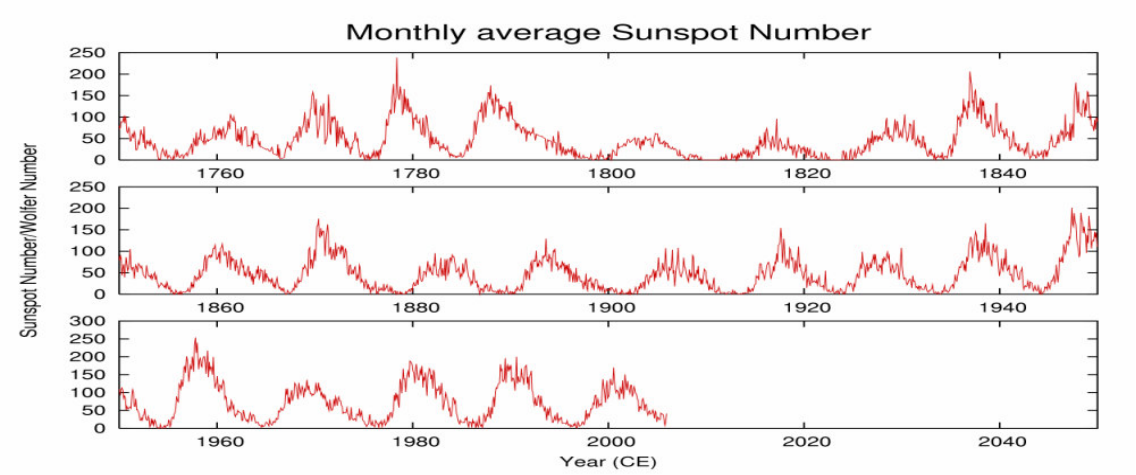

Figure 1.11. Distribution of the observed solar spot number (monthly averages) over the past 250 *years*

1.4 Evolution

1.4.1 Birth of the Sun

The Sun was born five billion years ago from the gravitational collapse of a hydrogen molecular cloud. One knows its age either from the general knowledge that we have accumulated on main sequence stars or by radiometric dating of the oldest isotopes of the solar system. Both methods give the same result, 4.57 billion years.

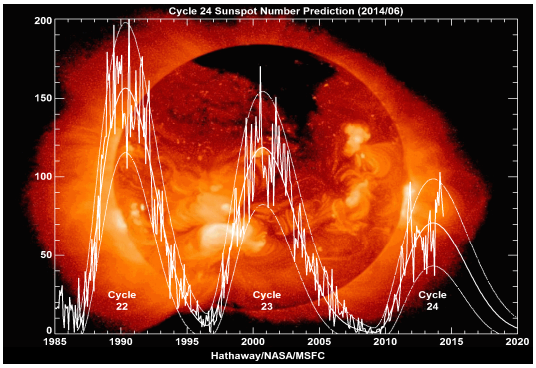

Figure 1.12. Sun spot numbers from 1985 up to now.

The Sun is essentially made of hydrogen and helium, amounting respectively to 74.8% and 23.7% of the mass inside the photosphere. The heavier elements, collectively called metals by astrophysicists, amount to less than 2% (0.8% of oxygen, 0.3% of carbon, 0.2% of neon and 0.2% of iron).

The Sun inherited these heavier elements from the interstellar matter of which it has been made. Hydrogen and helium are from the nucleosynthesis that followed the Big Bang by some 3 minutes; heavier elements were produced by stellar photosynthesis in the stars which died before the Sun was born. One takes it as granted that the chemical composition of the photosphere is the same as that of the primordial solar system. Yet, since its birth, the Sun has lost helium and heavy elements in its outer layers, which have migrated inward: the photosphere today contains less helium and only 84% of the heavy elements that were contained in the protostellar Sun (71.1% hydrogen, 27.4% helium and 1.5% metals).

1.4.2 Present phase

Available theoretical models that describe the evolution of the Sun tell us that three billion years ago the Sun luminosity was only 75% of the present luminosity. At that time it would then have been impossible to retain liquid water on the surface of the Earth and life could not have appeared as it did. However, geological data show that the Earth remained at more or less a same temperature during its whole history, if anything the young Earth was a bit warmer than it is today. It seems that the reason was a larger concentration of greenhouse gases in the atmosphere (CO_2, methane, ammoniac) which were keeping the heat to compensate the lesser Sun irradiance.

The Sun is about at the middle of its life, namely of its evolution on the main sequence. Each second, over four million tons of water are turned into energy within the solar core, producing neutrinos and photons. By now, the Sun already consumed some hundred solar masses. In total, it should spend some ten billion years on the main sequence.

In the Sun interior, nuclear fusion has modified the helium abundance which has now reached 60%. Of course, the metal abundance has not changed. As the Sun interior is radiative rather than convective, none of the fusion products had a chance to migrate outward to the photosphere. An important measure of heavy metal abundance is provided by meteorites, which never reached fusion temperature and are good witnesses of the composition of the protostellar Sun.

1.4.3 Death of the Sun

The Sun is not massive enough to end in a supernova explosion. Some five billion years from now, it will become a red giant, its outer envelope will expand at the same time as its core will contract and warm up (Figure 1.13). Helium will fuse into carbon when the temperature will reach some 100 MK.

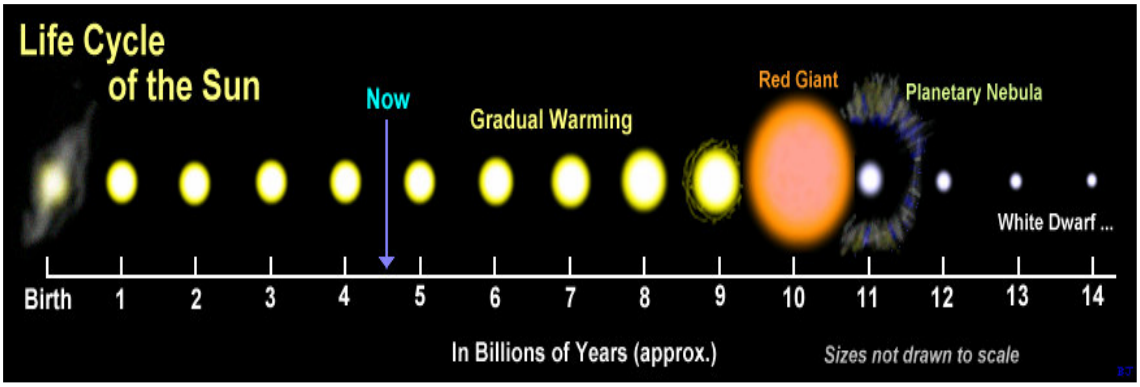

Figure 1.13. Schematic representation of the Sun evolution.

At the end of the red giant phase, large amplitude oscillations will eject the circumsolar envelope that will become a planetary nebula. The core will contract and become a white dwarf which will slowly cool down over billions of years.

2. DATA REDUCTION

The data used in the study had been collected between April and September 2012 and between October 2013 and January 2014 using the VATLY radio telescope [1, 2]. They were taken by tracking the Sun on-the-flight and have been used to study oscillations that were first reported [3] before being understood to be caused by multipathing [4]. As a by-product, flares had been identified that had been rejected from the oscillation analysis and which are the samples on which we have worked.

Reports on the performance of the telescope (Figure 2.1 left) are available [1] and [2]. Frequency spectra are made of three juxtaposed bandwidths covering together ~1.08 MHz in 138 bins of ~7.8 kHz each; the gain displays a small dependence on frequency, ~1.0 10^{-4}/kHz and a small non linearity reaching 6.2‰ on the Sun. Moreover, the gains of each of the three independent bandwidths fluctuate by 2 to 3‰ with respect to each other and are slightly higher in the centre of each bandwidth than on its edge, by typically 6‰, meaning an average correction of 2.6‰ on the Sun. The beam is well described by a Gaussian having a σ of 2.3° and the pointing accuracy is measured to be 0.22° in *acos(h)* and 0.11° in *h* where *a* and *h* are the azimuth and elevation respectively.

The flare sample includes 34 solar flares, 27 of which were detected during the second campaign of observations. The oscillation analysis was performed in parallel with that of data collected simultaneously at the same frequency (1415 MHz) by the Learmonth solar observatory [5] (Figure 2.1 right). Ha Noi and Learmonth are located at nearby longitudes (105.8°E and 114.1°E respectively) and at nearly opposite latitudes (21.0° N and 22.2° S respectively). The technical characteristics of the Learmonth radio telescope are essentially identical to those of the Ha Noi telescope, apart from the use of a linear rather than helical sensor, implying detection of the linear rather than circular component of the wave. The observatory is staffed seven days a week from sunrise to sunset and contributes data to the US Air Force Weather Agency, to the US National Oceanic and Atmospheric Administration and to the Global Oscillation Network Group. In addition to the 8' dish, it operates an 8.5 m dish (245 to 610 MHz), a 1 m dish (15.4 GHz), a swept frequency interferometric radiometer (30 to 80 MHz) and an optical telescope [1]. Its long experience with solar measurements and its commitment to serve a large community make it a highly reliable source of data. The noise level is a factor ~1.7 lower for the Learmonth radio telescope than for that in Ha Noi.

Figure 2.1. Left: the Ha Noi antenna. Right: the 8' and 1 m antennas in Learmonth.

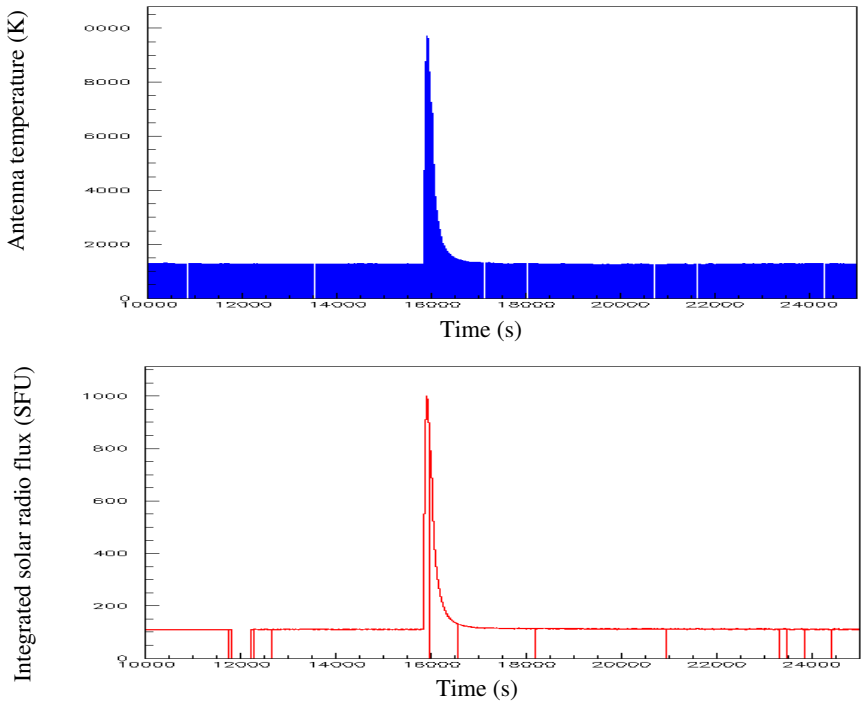

Figure 2.2. A typical flare: raw data for Ha Noi (up) and Learmonth (down). The abscissa is UT time in seconds. In the Learmonth case, there is in principle one measurement at each second. In the Ha Noi case, there is, in principle, one measurement every 8.2 s or so. The resolution of the picture prevents to see the fine structure that results and causes the area below the Ha Noi curve to be fully coloured. In both Learmonth and Ha Noi cases, one notes short periods during which measurements are missing.

The time dependence of the flux emitted by a typical flare is illustrated in Figure 2.2 that displays both the Ha Noi and Learmonth observations. Each measurement is averaged over the bandwidth of 1.08 MHz. The average is done for us in the Learmonth case, the data being available on the web [5] at 1 second intervals in solar flux units (1 SFU=10^4 Jy). In the Ha Noi case, they are calculated by us by averaging the 138 frequency channels of spectra such as that displayed in Figure 2.3. The Ha Noi data are collected in intervals of ~8.17 s and the measurement is of the antenna temperature. From [2], the conversion factor is 1.25 K/kJy.

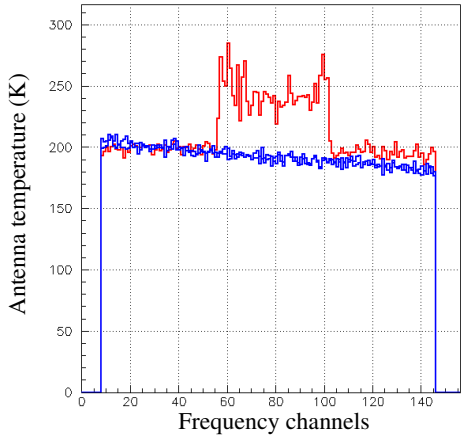

Figure 2.3. A typical frequency spectrum (blue). In some rare cases, as a result of man-caused interferences or of a transient on the power line, a spike occurs in the time distribution of the antenna temperature, associated with a dysfunction of the electronics as shown in red.

In both the Learmonth and Ha Noi data there are time intervals for which measurements are missing. The reason may be the need to recalculate a pointing correction or the presence of a man-caused interference causing a narrow spike, or the transient dysfunction of some electronics component. Moreover, in order to compare Learmonth and Ha Noi data, we decided to use a common time scale in bins of one second. This implied, for each time value (in a sequence of 1 s intervals) to interpolate the Hanoi measurements. The result obtained in the case of the flare illustrated in Figure 2.2 is displayed in Figure 2.4 left.

At that stage, we define by eye two time limits, t_1 and t_2, bracketing the flare and we use the flux distribution outside these limits to fit a linear background describing the Sun emission before and after the occurrence of the flare. We use it to define the flare flux, S_{flare}, integrated between t_1 and t_2 and background subtracted, and the mean quiet Sun emission during the flare, S_{quiet}, defined as the value taken by the linear background at time $t_{average}=½(t_1+t_2)$. The procedure is illustrated in Figure 2.4 right.

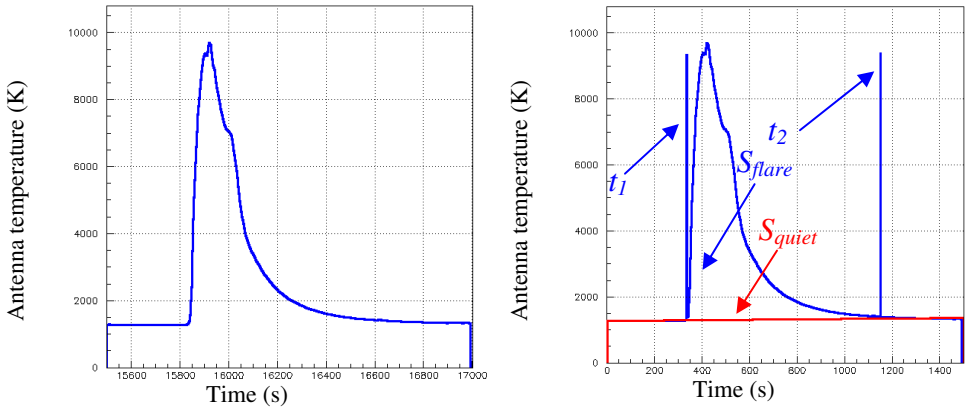

Figure 2.4. Left: the flare displayed in Figure 2.2 (Ha Noi data) after conversion to 1 s bins and interpolation across missing measurements. Right: the same showing the limits t_1 and t_2 and the linear background (red).

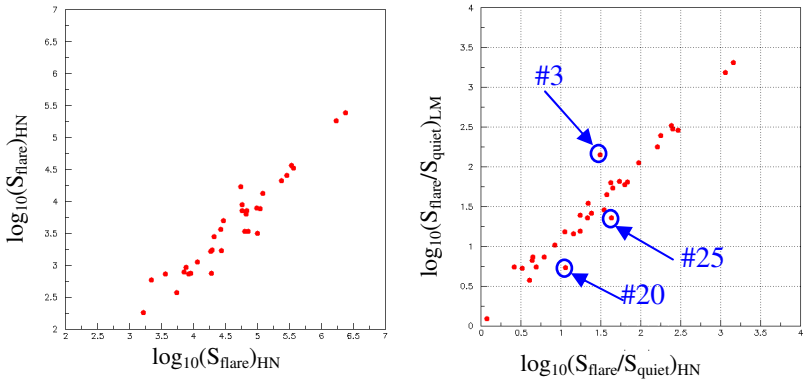

Figure 2.5. Left: scatter plot of S_{flare} in the Learmonth (ordinate) vs Ha Noi (abscissa) plane. The quantities plotted are $\log_{10}(S_{flare})$. Right: same, with the quantities plotted being $\log_{10}(S_{flare}/S_{quiet})$.

The scatter plot of S_{flare} in the Learmonth/Ha Noi plane is shown in Figure 2.5 left. It shows an important dispersion that is significantly reduced when normalizing S_{flare} to S_{quiet}, showing that much of the dispersion is due to gain drifts rather than different levels of the background sky in Ha Noi and Learmonth (Figure 2.5 right). Indeed, a change of gain affects S_{flare} and S_{quiet}, in the same way and leaves their ratio invariant, while a change in sky background level affects only S_{quiet}. This is made more visible in Figure 2.6 left by plotting the distribution of

$log_{10}(0.1S_{flare,Ha\ Noi}/S_{flare\ Learmonth})$. The same distribution with the values of S_{flare} normalized to S_{quiet} is displayed in Figure 2.6 right. Flares 6 and 24 are found to be associated with wrong gain values in the Ha Noi measurement, resulting in anomalous quiet Sun levels. However, flares 3, 20 and 25 stand out as displaying non trivial disagreements between the Ha Noi and Learmonth measurements.

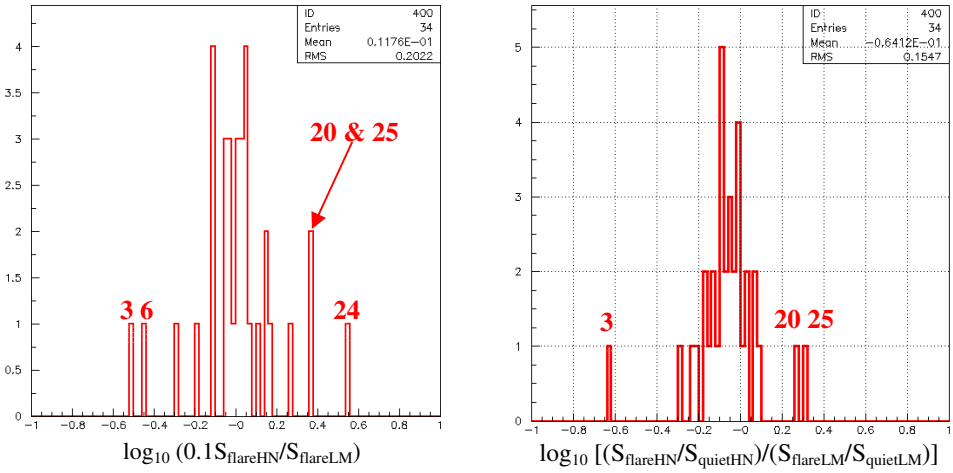

Figure 2.6. Left: distribution of $\log_{10}(0.1S_{flare,Ha\ Noi}/S_{flare\ Learmonth})$. Right: same distribution with the values of S_{flare} normalized to S_{quiet}.

The last step consists in normalizing the flare flux distributions to a common flux scale by dividing the measured fluxes by the associated values of S_{flare}. The result is displayed in Figure 2.7 for the flare of Figure 2.2. It is then possible to define a χ^2 measuring the quality of the agreement between the Ha Noi and Learmonth measurements (here χ^2 is simply the sum of the squared differences between the two measurements over the $[t_1, t_2]$ interval). However, before doing so, we optimize the time delay Δt to be applied to the Learmonth data with respect to the Ha Noi data by minimizing the associated value of χ^2. We expect the best fit value of Δt to cancel within ~ ±4 s. Its mean value is 1.8 s and the rms 3.9 s. The results are listed in Table 2.1 for each of the 34 flares. The distributions of Δt and χ^2 are displayed in Figure 2.8 and studied in the next chapter.

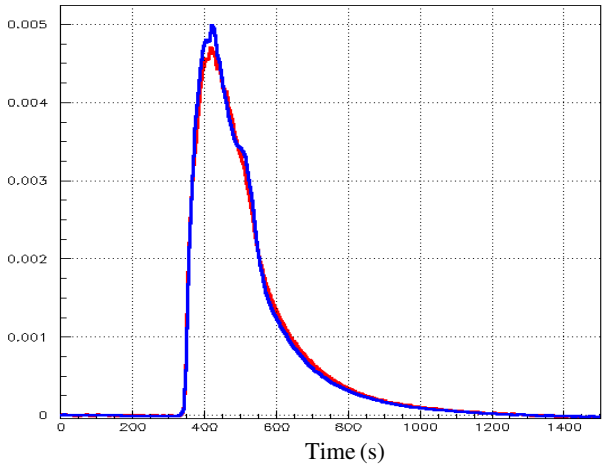

Figure 2.7. The flare of Figure 2.2 after normalisation to unit area between t_1 and t_2. Ha Noi data are shown in blue and Learmonth data in red.

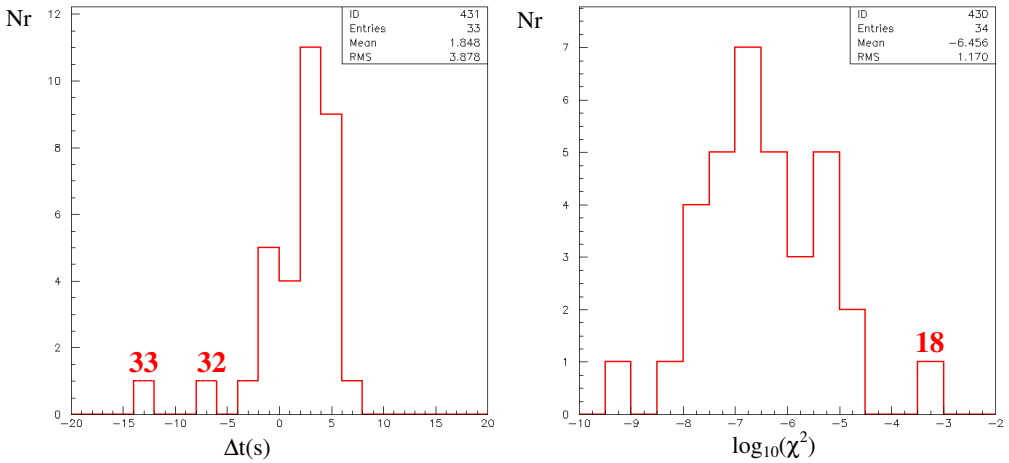

Figure 2.8. Left: distribution of the best fit Δt values. Right: distribution of the best fit values of $\log_{10}(\chi^2)$ where χ^2 has been divided by the width of the flare interval, t_2-t_1.

Table 2.1 Parameters of the 34 selected flares

Nr	Date	S_{flare}		S_{quiet}		Δt (s)	$log_{10}(\chi^2)$
		Learmonth $(SFU * s) \times 10^3$	Ha Noi $(K*s) \times 10^3$	Learmonth (SFU)	Ha Noi (K)		
1	131025_01	6.4	64.2	115.8	1407	4	–6.8
2	131025_02	244.7	2364.0	117.9	1511	–4	–6.8
3	131025_03	16.2	50.5	117.9	1534	3	–6.1
4	131026_01	7.4	106.6	114.8	1610	2	–6.3
5	131028_01	35.8	342.3	116.1	1358	4	–6.8
6	131029_01	0.6	2.2	112.2	778	2	–4.3
7	131102_01	1.1	12.2	111.0	1501	3	–4.9
8	131103_01	0. 4	5.6	107.0	1307	6	–4.4
9	131105_01	1.7	18.0	109.6	1404	1	–3.9
10	131106_01	1.8	26.3	114.1	1449	5	–5.3
11	131106_02	0.8	6.8	109.8	1434	4	–4.8
12	131107_01	20.8	234.0	109.7	1308	2	–5.9
13	131108_01	0.7	8.7	109.9	1305	3	–4.1
14	131108_02	188.2	1685.3	115.4	1315	1	–6.4
15	131110_01	25.7	285.4	110.4	1382	2	–5.7
16	131112_01	7.7	98.4	125.8	1519	4	–6.1
17	131113_01	1.6	18.7	120.4	1397	2	–5.8
18	131117_01	0.2	1.7	142.4	1627	6	–3.0
19	131118_01	0.8	8.9	139.6	1541	5	–4.5
20	131118_02	0.8	18.1	134.4	1566	–2	–5.5
21	131207_01	35.0	378.0	123.5	1465	–1	–7.4
22	131212_01	3.6	28.1	148.0	1554	5	–6.5
23	131215_01	0.7	3.7	130.0	1117	2	–4.3
24	140101_01	3.0	105.2	111.1	4277	2	–5.8

25	140108_01	3.2	76.7	143.2	1822	–1	–5.9
26	140110_01	0.9	7.9	132.8	1731	2	–5.4
27	131117_02	6.7	69.2	143.7	1738	5	–6.4
28	120427_01	8.0	60.5	121.8	1083	0	–6.8
29	120507_01	2.6	20.2	122.8	953	–2	–4.9
30	120703_01	34.3	363.5	116.4	1254	4	–4.9
31	120706_01	12.8	121.4	116.4	1231	–1	–5.3
32	120709_01	4.8	30.4	133.4	1377	–7	–5.5
33	120710_01	8.0	63.0	139.5	1571	–13	–4.6
34	120904_01	3.4	62.4	122.2	1866	0	–5.5

3. DETAILED STUDY OF THE FLARE SAMPLE: COMPARISON OF LEARMONTH AND HANOI

From Figures 2.6 and 2.8 we note the presence of 8 flares that depart significantly from average behaviour. Their parameters are listed below.

Table 2.2 Parameters of the 8 anomalous flares

Nr	Date	S_{flare}		S_{quiet}		Δt (s)	$log_{10}(\chi^2)$
		Learmonth $(SFU*s)\times10^3$	Ha Noi $(K*s)\times10^3$	Learmonth (SFU)	Ha Noi (K)		
3	131025_03	16.3	50.5	118	1534	3	–6.1
6	131029_01	0.61	2.18	112	778	2	–4.3
18	131117_01	0.18	1.74	142	1627	6	–3.0
20	131118_02	0.77	18.1	134	1566	–2	–5.5
24	140101_01	2.96	105	111	4277	2	–5.8
25	140108_01	3.22	76.7	143	1822	–1	–5.9
32	120709_01	4.76	30.4	133	1377	–7	–5.5
33	120710_01	8.07	63.0	140	1571	–13	–4.6

Flare #18 is a very small flare and has the highest value of χ^2. Figure 3.1 compares its profiles in the Ha Noi and Learmonth data. It is a typical case of fine structure occurring at a time scale of 1 second, to which the Ha Noi data are blind because of the averaging time of 8 seconds.

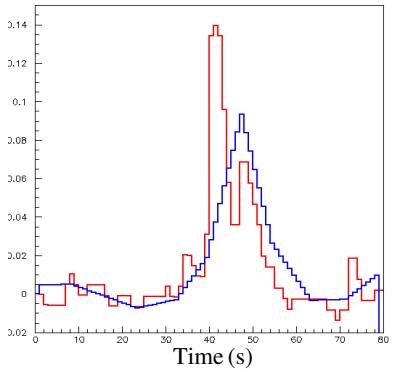

Figure 3.1. Profiles of flare #18 as measured in Ha Noi (blue) and Learmonth (red). The interpolation performed between successive Ha Noi measurements is clearly visible.

3.1 Flares showing a time shift

Flares #32 and #33 have the lowest values of Δt, −7 s and −13 s respectively. What happens there is in fact an artefact that is well illustrated by the case of flare # 33 as displayed in Figure 3.2. The raw data start clearly together, consistent with $\Delta t \sim 0$. However, they depart from each other after some time. When adjusting the value of Δt, we first normalize the two flares to a same area, which artificially causes the Ha Noi flare to start before the Learmonth flare. We note that the quiet Sun level after the flare remains higher in the Learmonth data than in the Ha Noi data. Indeed, Figure 3.3 shows that across the flare the Ha Noi electronics was somewhat disturbed; it is as if this disturbance would still have some effect on the gain after the flare. Flare #32, illustrated in Figure 3.4, suffers from the same disease as flare # 33.

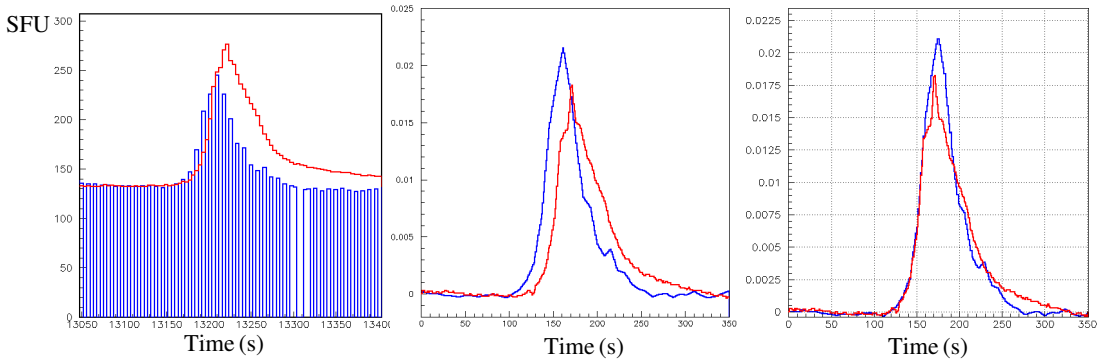

Figure 3.2. Left: Raw data for flare #33, Ha Noi (blue) and Learmonth (red), normalized to a same quiet Sun level before the flare (time bins of 4 s). Middle: the two flares are normalized to a same area before adjusting Δt. Right: Good, but artificial, agreement is then obtained by shifting the flares in time with respect to each other.

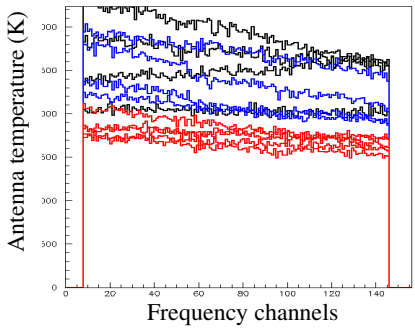

Figure 3.3. Frequency spectra measured in Ha Noi when crossing flare # 33. Before and after the flare is displayed in red, on the rise in black and on the fall in blue.

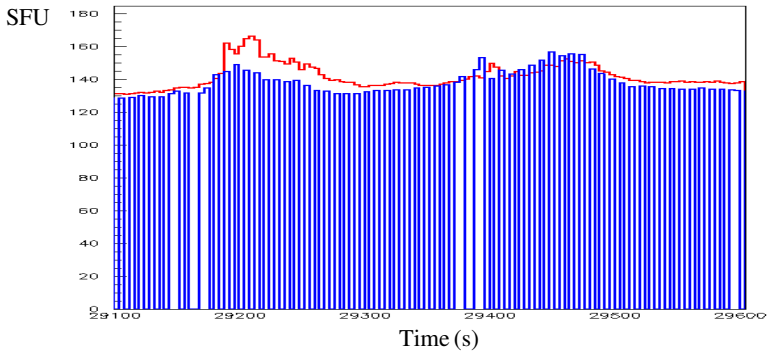

Figure 3.4. Raw data for flare #32, Ha Noi (blue) and Learmonth (red), normalized to a same quiet Sun level before the flare (time bins of 4 s).

The raw data of flare #32 are displayed in Figure 3.4. Here again, the shift is an artefact of the disagreement between the fluxes of the first peak as measured in Learmonth and Ha Noi. However, the frequency slopes across the peak are well behaved in this case.

3.2 Flares having different integrated fluxes

Flares # 3, 6, 20, 24 and 25 show a poor agreement between the Ha Noi and Learmonth measurements of the integrated flux. Their profiles are displayed in Figure 3.5. We know [2] that in cases of very large signals, and/or of rapidly changing fluxes, the Ha Noi measurements are ill -behaved with frequency spectra displaying anomalous slopes. This is the case of flare #2, the strongest flare in the sample, the slope and the structure of the frequency spectrum displaying clear dysfunctions on the peak as shown in Figure 3.6. However, in the case of the flares under consideration in the present section, the frequency spectra remain well-behaved when scanning across the peak of the flare as illustrated in Figure 3.7. The disagreement observed with flares #6 and 24 disappears when normalizing to quiet Sun level and can be blamed on a wrong gain in the Ha Noi measurement. Indeed, flare #6 has a quiet Sun level and a calibration constant twice as small as usual and flare #24 a quiet Sun level four times as large as usual.

The cases of flares #3, 20 and 25 stand out as displaying a disagreement between the Learmonth and Ha Noi fluxes that subsists when normalizing to the quiet Sun level, as illustrated in Figures 2.5 right and 2.6 right.

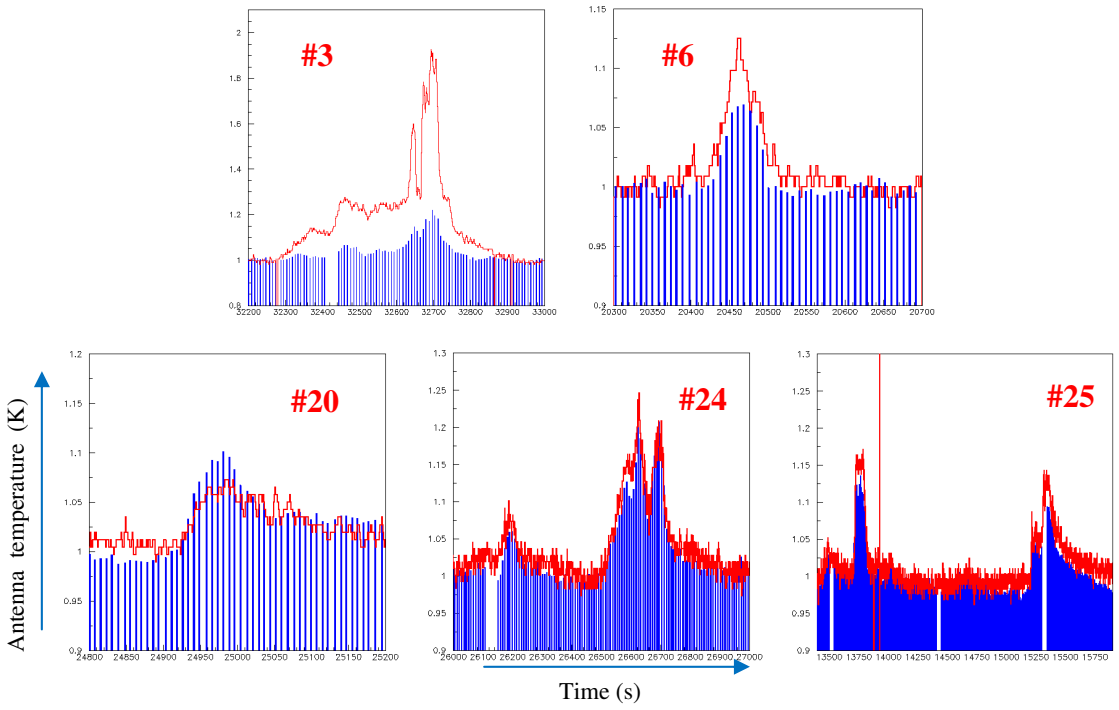

Figure 3.5. Raw data normalized to quiet Sun level for 5 flares displaying disagreement between Ha Noi (blue) and Learmonth (red). The time span is $[t_1, t_2]$ and the bin width is 1 s.

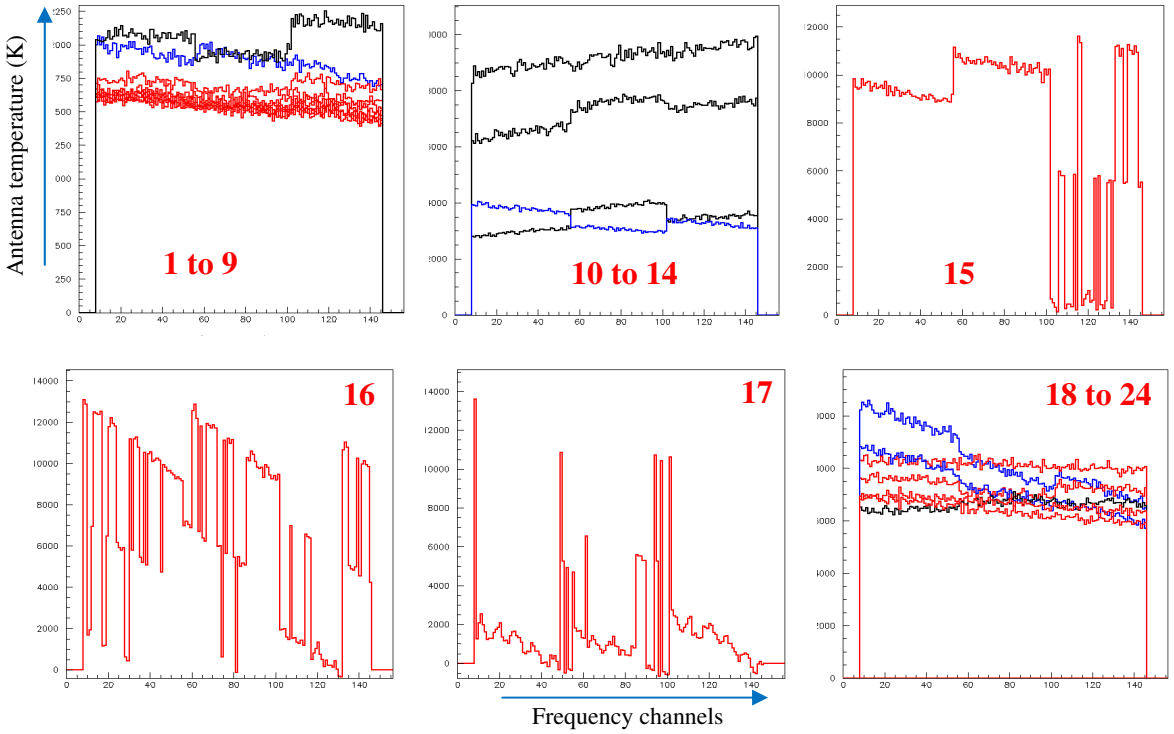

Figure 3.6. Twenty four successive frequency spectra covering the peak of the flare #2. 1 to 7 (red); 8(blue); 9(black); 10 (black); 11(blue); 12 to 14(black); 15, 16, 17 (red); 18 (blue); 19, 20 (red); 21 (blue); 22 (black); 23 and 24 (red);

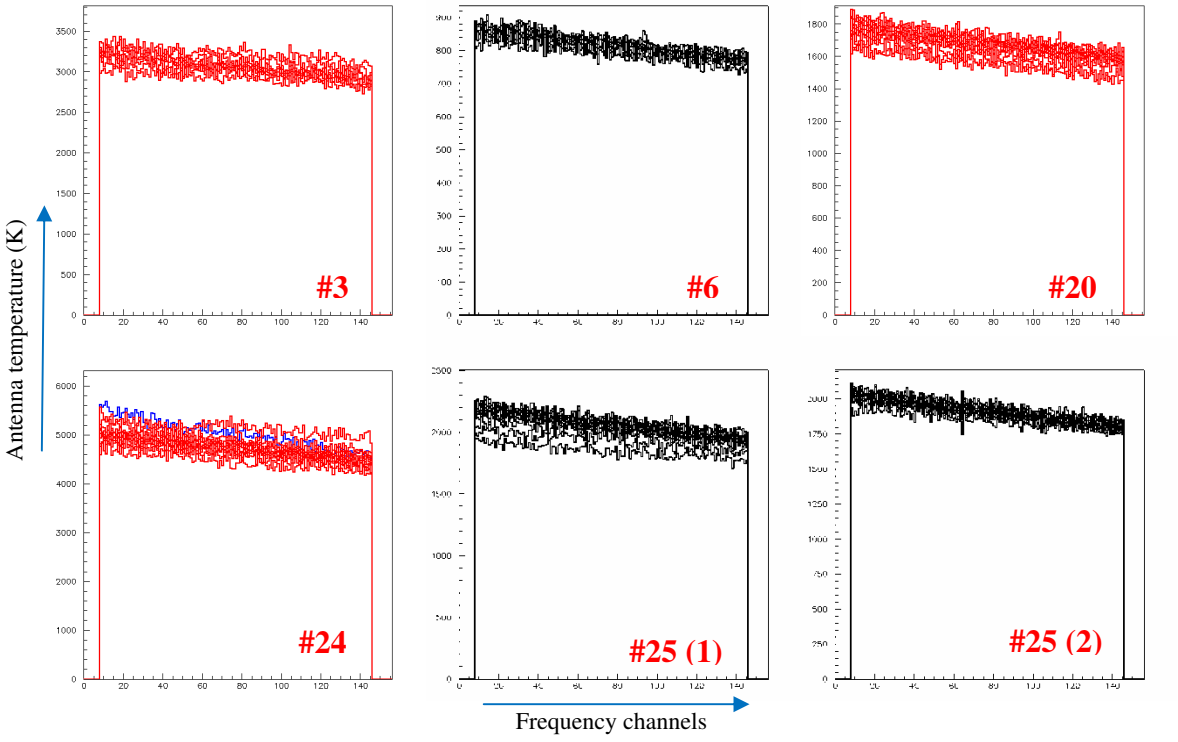

Figure 3.7. Frequency spectra covering the peaks of flares having different integral fluxes in the Ha Noi and Learmonth data (flare # 25 has two peaks)

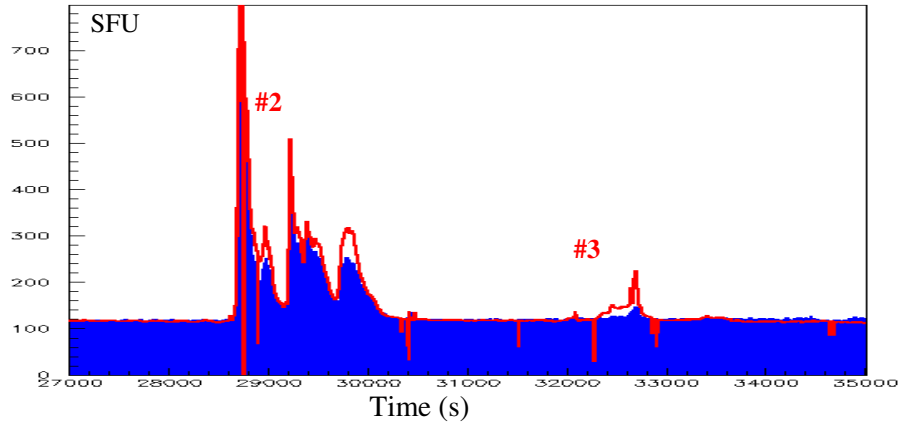

Figure 3.8. Comparison between the Learmonth (red) and Ha Noi (blue) measurements on flares # 2 and 3. Fluxes have been normalized to quiet Sun level.

The case of flare #3 is illustrated in Figure 3.8. It occurs about an hour after the very big flare #2. The Ha Noi data are already lower than the Learmonth data in the third peak of flare #2; could the electronics heat up and take so long to cool down? This does not seem a reasonable assumption; it is very difficult to imagine a mechanism that would remember flare #2 one hour later. If it were a non instrumental effect, we can only think of polarization (the Ha Noi and Learmonth sensors select different polarizations, circular and linear respectively). Disturbances of the ionosphere following the X - ray flux should not affect radio waves at our high frequency of 1415 MHz. We meticulously looked at all features of the Ha Noi flare #3 data and did not find anything abnormal. We are unable to explain the much lower flare #3 fluxes observed in Ha Noi than in Learmonth. On the contrary, flares # 20 and 25 are understood as simply marginal cases as seen on Figures 2.6 left and 3.5 and do not raise major questions.

3.3 Main features

Figure 3.9 displays the 34 profiles as measured in Ha Noi and in Learmonth after subtraction of the quiet Sun level and normalization to unit integral flux. We note that some flares consist of a single peak while others display a sequence of peaks. Flares of the first kind usually have a fast rise time and a slow fall time, sometimes displaying a hint for a second peak. Other flares display two clean peaks while the rest of the sample displays a sequence of peaks. Two thirds of the single peak sample (8 out of 12 flares) have a full width at half maximum (FWHM) just below one minute and span more than 1.5 orders of magnitude in integral flux. The one third of the single peak sample (4 out of 12 flares) have FWHM values between 1.5 minutes and 3 minutes and integral fluxes larger than average. Double peak flares have much larger FWHM values than single peak flares, over 3 minutes on average, consistent with the idea that they are made of a succession of flares similar to those of the single peak sample. In order to quantify these observations, we define for each flare a duration D (in minutes) and a number of peaks P listed in Table 3.1 together with the value of $L=log(S_{flare})$. There is much subjectivity and some arbitrariness in the definitions of P and D. In particular, when a peak is not clearly resolved but shows up as simple shoulder on another peak, it is counted as one half.

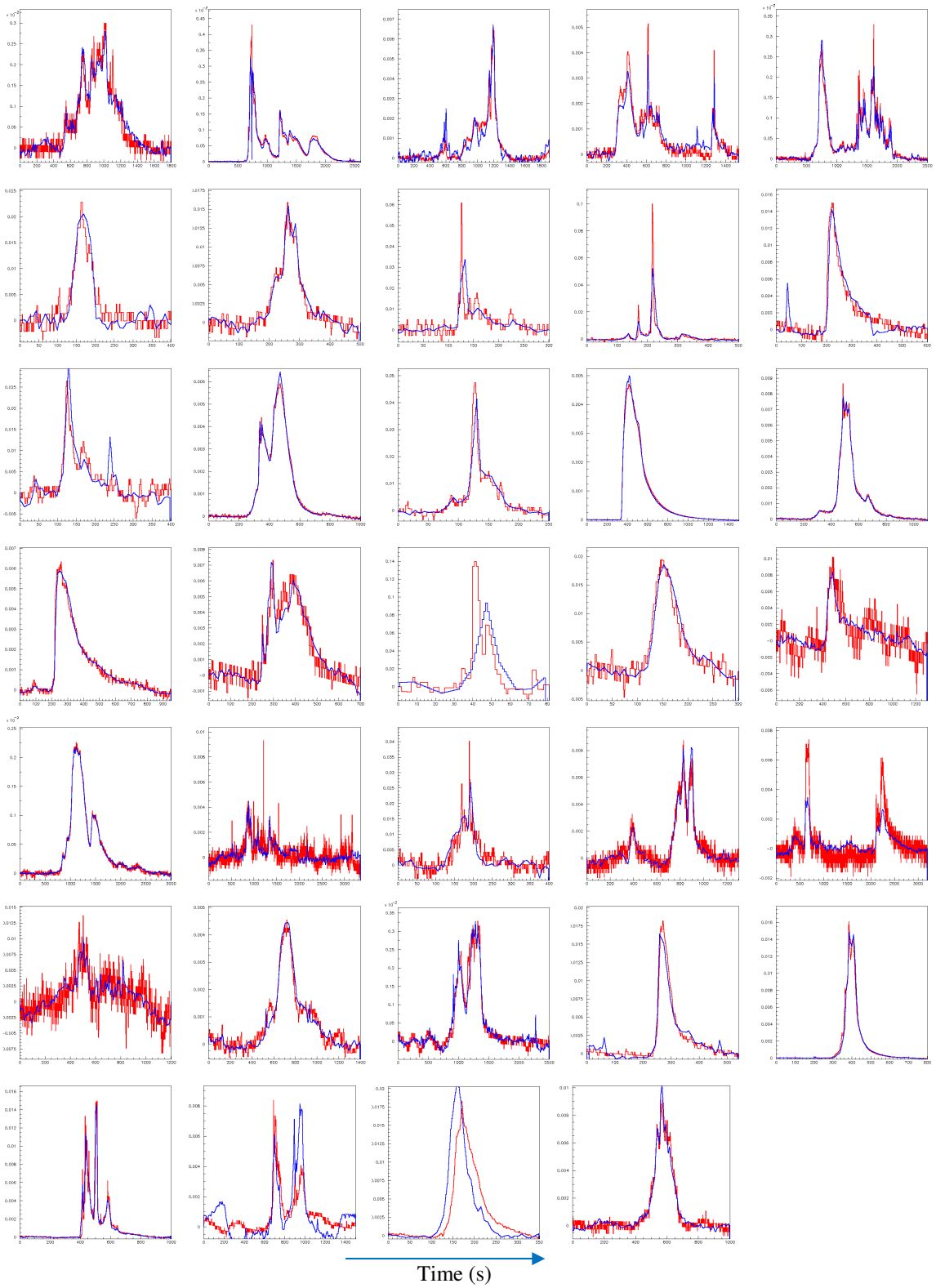

Figure 3.9. Profiles of the 34 flares, quiet Sun subtracted and normalised to unit integral flux. Hanoi data are shown in blue and Learmonth data in red. Flare numbers are in sequence from left to right and from up to down.

Table 3.1 The values of *P, L* and *D* of the 34 selected flares

#	1	2	3	4	5	6	7	8	9	10	11	12	13	14	15	16	17
D	17.5	22.5	13.3	19.2	21.7	1.3	2.5	2.5	4.5	3.3	2.8	7.5	2.3	10.8	7.5	11.0	5.0
P	6	5	4	5	5	1	1.5	3	4	1	3	2	2.5	1	3	1	2.5
L	3.8	5.4	4.2	3.9	4.6	2.8	3.1	2.6	3.2	3.2	2.9	4.3	2.9	5.3	4.4	3.9	3.2
#	18	19	20	21	22	23	24	25	26	27	28	29	30	31	32	33	34
D	0.3	2.5	12.5	20.0	21.7	2.5	13.3	41.7	17.5	11.7	10.0	3.3	3.7	3.7	7.5	3.2	5.0
P	1	1	3	2	3	2	3.5	4.5	5	1	2	1	1.5	3	2.5	1	1
L	2.3	2.9	2.9	4.5	3.6	2.9	3.5	3.5	3,0	3.8	3.9	3.4	4.5	4.1	3.7	3.9	3.5

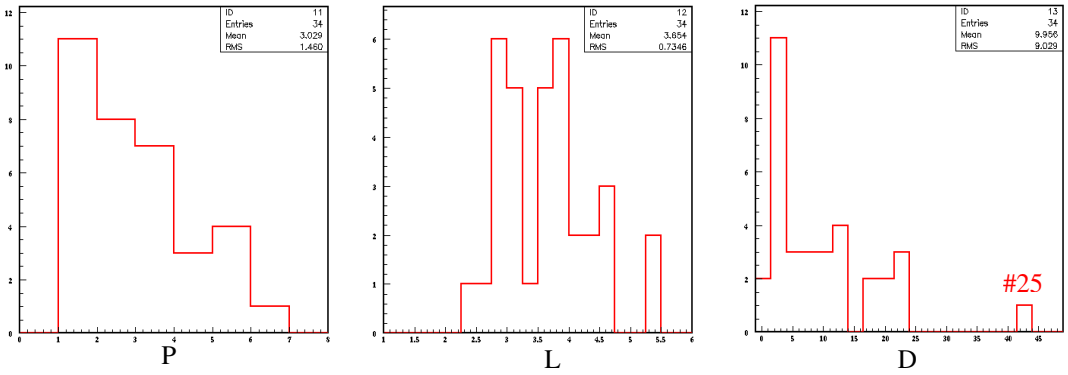

Figure 3.10. Distributions of P (left), L (centre) and D (right) for the sample of 34 flares.

The distributions of the three quantities *P*, *D* and *L* are displayed in Figure 3.10 and the correlations between them in Figure 3.11. The number of peaks has a mean value of ~3 and has a smoothly decreasing distribution with about one third of the sample being single peaks. The variable *L* has a broad distribution and *D* displays a peak at short durations with 13 flares having a mean duration of 2.6 min with little dispersion. Flare #25 stands out as having a particularly long duration but it is in fact made of two shorter flares, with typical durations of 2 to 3 min for the first and 10 to 15 min for the second with some 25 min between them. While there is no correlation between the number of peaks and the integral flux, both the number of peaks and the integral flux increase with duration, supporting the idea that many flares are in fact a succession of shorter flares.

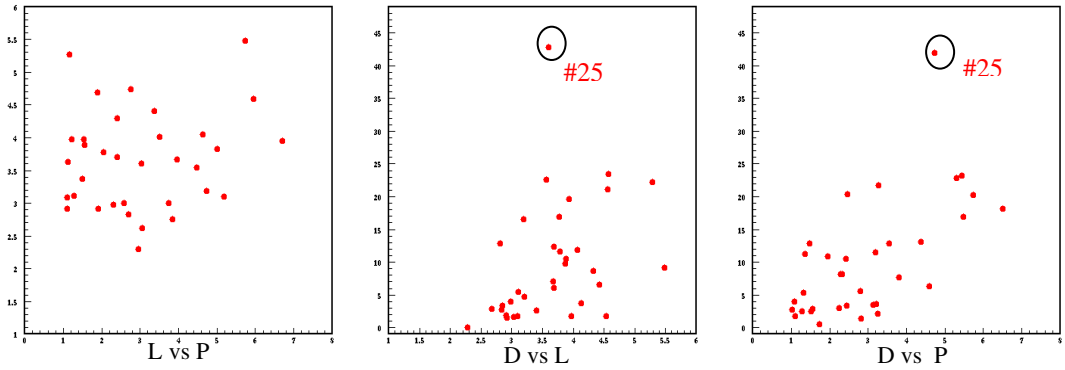

Figure 3.11. Left: Correlations between L (ordinate) and P (abscissa); centre, between D and L; right, between D and P.

4. CONCLUSION

We have examined a sample of 34 solar flares collected using the VATLY radio telescope at 1415 MHz frequency and we have compared them with measurements made in Australia by the Learmonth solar observatory. In general the two samples display a good agreement given the difference in time resolution (1 s in Learmonth and 8.2 s in Ha Noi). A few cases of important disagreement of the measured fluxes have been identified and explained, with the exception of a small flare occurring one hour after the largest flare in the sample for which the flux measured in Ha Noi is much smaller than that measured in Learmonth with no obvious reason. Other, less spectacular cases of flares starting together in Ha Noi and Learmonth but deviating from each other after some fraction of the rise time have been observed without having been understood. The main causes of disagreement are to be blamed on the Ha Noi data: wrong gain evaluation, disturbances of the electronics response in cases of very large signals, worse time resolution (8 s rather than 1 s). Flares are seen to be often reducible to a sequence of peaks as illustrated by the correlations observed between their duration on one side and their integral flux and number of peaks on the other side.

ACKNOWLEDGEMENTS

I am grateful to Prof. Pierre Darriulat, without him this report is impossible.

I would like to thank Dr. Nguyen Thi Thao, Dr. Pham Ngoc Diep, Nguyen Thi Phuong and other staff members in VATLY. They welcomed me warmly during my stay and helped me a lot to understand and fulfil my work.

I would like to acknowledge USTH and INST for their constant support.

Finally, I also deeply thank all my friends who shared with me joys and sorrows in the work.

REFERENCE

[1] N.V. Hiep *et al.*, *The VATLY radio telescope*, 2012, Comm. Phys. Vietnam, Vol 22, No 4 (2012) page: 365-374.

[2] N.T. Phuong *et al.*, 2014, *The VATLY radio telescope: performance study*, accepted for publication in Comm. Phys. Viet Nam.

[3] N.V. Hiep *et al.*, *Radio Observation of Solar-Activity-Related mHz Oscillations*, 2014, Solar Physics 289, 3, 939.

[4] P. N. Diep *et al.*, *Correlated oscillations due to similar multi-path effects seen in two widely separated radio telescopes*, 2014, PASA, 31, e029.

[5] Australian Government, Bureau of Meteorology, Radio and Space Weather Services, http://www.ips.gov.au/World_Data_Centre/1/10.